CANCER DIAGNOSIS & PROGNOSIS
4: 544-557 (2024) doi: 10.21873/cdp.10362

Review

The Role of Microsurgery and Fluorescent-reporter Genes in Establishing Mouse Models for Real-Time Imaging of Metastatic Cancer-Cell Trafficking and Colony Formation: A Revolutionary and Disruptive Technology for Metastasis Research

SEI MORINAGA[1,2,3], NORIO YAMAMOTO[3], KENSUKE YAMAUCHI[3], KATSUHIRO HAYASHI[3], HIROAKI KIMURA[3], SHINJI MIWA[3], KENTARO IGARASHI[3], TAKASHI HIGUCHI[3], HIROYUKI TSUCHIYA[3], SATORU DEMURA[3] and ROBERT M. HOFFMAN[1,2]

[1]*AntiCancer Inc., San Diego, CA, U.S.A.;*
[2]*Department of Surgery, University of California, San Diego, CA, U.S.A.;*
[3]*Department of Orthopedic Surgery, Graduate School of Medical Sciences, Kanazawa University, Kanazawa, Japan*

Abstract. *The field of experimental microsurgery was pioneered by the great microsurgeon Sun Lee, who developed the foundation of transplant surgery in the clinic. Dr Lee also played a seminal role in introducing microsurgery to establish mouse models of cancer. In 1990, at the age of 70, Dr Lee demonstrated microsurgery techniques to the mouse-model team at AntiCancer Inc., leading to the development of the surgical orthotopic implant (SOI) technique and the first orthotopic mouse models of cancer that metastasized in a pattern similar to clinical cancer. At the beginning of the present century, one of us (NY) from Kanazawa University School of Medicine became a visiting scientist at AntiCancer to learn SOI and develop mouse models of cancer using cancer cells expressing fluorescent reporter genes, such as green fluorescent protein (GFP) and red fluorescent protein (RFP), in order to image metastatic cancer cells trafficking in real time. Since then, a total of eight young surgeons from Kanazawa University have been visiting researchers at AntiCancer, developing SOI mouse models of cancer to visualize cancer cells in vivo, tracking all stages of metastasis in real time. The present perspective review summarizes this seminal work, which has revolutionized the field of metastasis research.*

Correspondence to: Robert M. Hoffman, Ph.D., AntiCancer Inc, 7917 Ostrow St, Suite B, San Diego, CA, 92111, U.S.A. Tel: +1 6198852284, e-mail: all@anticancer.com

Key Words: Microsurgery, mouse models, orthotopic, surgical orthotopic implantation, SOI, metastasis, fluorescent reporter gene, GFP, RFP, cancer-cell trafficking, cancer-cell-immune-cell interaction, imaging, real time, review.

In 1969, one of the most important discoveries in the history of cancer research was made: athymic nude *nu/nu* mice could support the growth of human cancer cells (1). Until this discovery, there was no systematic experimental animal system to study human cancer. The nude mouse was subsequently demonstrated to enable growth of all types of human cancer cell lines as well as patient tumors (2). The initial nude-mouse cancer models involved subcutaneous implantation, in which metastasis rarely occurred (2). Sordat *et al.* (3) established the first orthotopic nude mouse model by injection of colon cancer cells into the colon of nude mice, which demonstrated cancer-cell invasion, but no metastasis.

Our laboratory began to develop orthotopic nude mouse models in the late 1980's (4). In 1990, a breakthrough occurred when Dr. Sun Lee, the pioneer of experimental microsurgery (5), visited the laboratory at AntiCancer Inc. to demonstrate microsurgery on mice. This technique involved implanting tumor fragments, either from clinical sources or grown subcutaneously in nude mice, into the corresponding organs of other nude mice. This method became known as surgical orthotopic implantation (SOI) and led to clinical transplantation of tumors to the liver, kidney, lung, colon, breast and other organs.

Very soon, surprising results were obtained where a bladder cancer cell line was shown to be highly metastatic when transplanted by SOI in the bladder, compared to when cell suspensions were injected into the bladder (6, 7). Similar results of high rates of metastasis were observed with SOI nude mouse models of the lung (8), breast (9), ovary (10), pancreas (11), colon (12), and prostate (13).

Another breakthrough occurred in the AntiCancer Laboratory when it was discovered that cancer cells expressing the jelly fish green fluorescent protein (GFP) could be imaged *in vivo*, even non-invasively (14, 15).

At this time in 2001, one of us (NY) arrived at AntiCancer to develop imageable SOI metastatic models using GFP. The initial results and those of subsequent scientists from Kanazawa University visiting AntiCancer, are summarized below. These findings led to the development of new disruptive and revolutionary technology for the study of metastatic cancer.

Determining Clonality of Metastases in the Lungs of Mice With Fluorescent Reporter Gene

Mixtures of GFP- and red fluorescent protein (RFP)-expressing HT1080 fibrosarcoma cells were injected into the tail vein (experimental metastasis) or foot pad (spontaneous metastasis) of nude or SCID mice. Colonies that developed in the lung that were pure GFP or pure RFP, were considered clonal. Colonies of mixed GFP and RFP fluorescence were considered not clonal. Rare spontaneous lung metastasis that arose after foot-pad injection were mostly single color, thereby clonal. The frequent lung colonies arising after tail-vein injection of cell mixtures were predominantly of mixed color, not clonal. These results suggested that rare lung metastases, which are the usual clinical pattern, are clonal (Figure 1A-C) (16, 17).

Imaging Metastatic Progression in the Lung With GFP- and RFP-expressing Cancer Cell Lines in Real Time

Similar to the experiments described above, mixtures of GFP and RFP cancer cells were injected into the tail vein or foot pad to develop experimental or spontaneous metastasis, respectively, but in this case to image metastatic progression in real time. Imaging was performed by visualizing the colonies growing in the lung *via* a skin flap over the transparent chest wall. Pure and mixed colonies growing in the lung could be seen growing in real time, indicating clonal and non-clonal metastasis, respectively (Figure 2A and B, Figure 3A-F) (17-19).

Imaging Nuclear-cytoplasmic Dynamics of Cancer Cells Expressing GFP in the Nucleus and RFP in the Cytoplasm Trafficking in Microvessels in the Brain

After common-carotid-artery injection in nude mice, cancer cells expressing GFP in the nucleus and RFP in the cytoplasm were visualized through the transparent skull with a skin flap in the scalp, in micro vessels in the brain trafficking in single-file. Both the nuclei and cytoplasm appeared deformed, and the cancers cells became elongated in order to traffic in the very narrow micro vessels of the brain. The dual-color cancer cells were so bright, that a mitotic cell could be imaged non-invasively in the ear of the mouse with the nuclei and cytoplasm of the 2 cells clearly distinguishable (Figure 4A-C) (20).

Imaging of Narrow-vessel Trafficking of Deformed Cancer Cells Labeled in the Nucleus With GFP and Cytoplasm With RFP in the Abdominal Area

With cancer cells labeled with GFP in the nucleus and RFP in the cytoplasm, it was possible, after injection of the cells into the heart, to visualize the dynamics of nuclear and cytoplasmic deformation, as well as the velocity of cancers cells trafficking in various-sized vessels in the inside surface of an abdominal skin flap. Before cancer-cell injection, the epigastrica cranialis vein in the skin flap was closed with a 6-0 suture.

The cytoplasm and nuclei of the cancer cells elongated to fit within the capillary they occupied. The cytoplasm could deform extensively, up to four times its normal length, and could fracture if the deformation was too extensive. The nuclei were more rigid and much less deformable than the cytoplasm and could extend to only 1.6 times their normal length, in narrow capillaries. In capillaries of approximately 8 μm in diameter, cancer cells could migrate 48.3 μm/h. The minimum capillary diameter that allowed cell migration was approximately 8 μm (Figure 5A-G) (21).

Imaging the Process of Extravasation of Dual-color Cancer Cells, With GFP in the Nucleus and RFP in the Cytoplasm, in Vessels Where they Are Trafficking

Cancer cells expressing GFP in the nucleus and RFP in the cytoplasm were injected through a vascular route in an abdominal skin flap and imaged in real time. The cancer cells migrated by various means in the vessels or adhered to the vessel walls and some adhered to the vessel outer surface surface after extravasation. During extravasation the cancer cells exited the vessels with the nuclei following a cytoplasmic projection that perforated the blood vessel to begin the exit process from the vessel. Both cytoplasm and nuclei underwent deformation during extravasation. Extravasation was rare for HT1080-GFP-RFP-cells but frequent for the mouse mammalian tumor cell line MMT-GFP-RFP. The trafficking cancer cells were observed to aggregate, and aggregates could collide and adhere to each other in large vessels. Cancer cells migrated at 24 μm/second in large vessels.

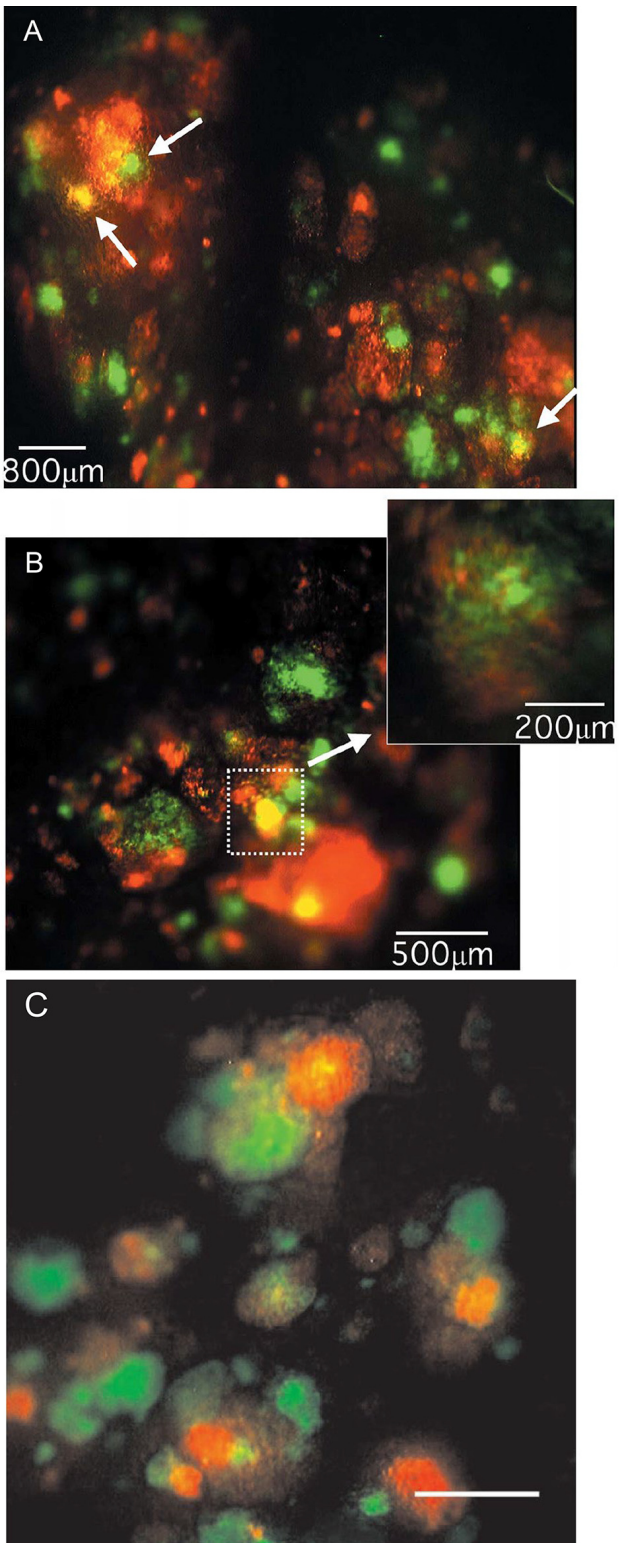

Figure 1. *Images of clonal and non-clonal lung metastase after tail-vein co-injection of HT-1080-RFP and HT-1080-GFP cells. A, B, C) High-magnification fluorescence images showing color-coded metastatic colonies in the lung. Most colonies are dual-color and, thereby, non-clonal (arrows) (16, 17). Bar in C 1 mm.*

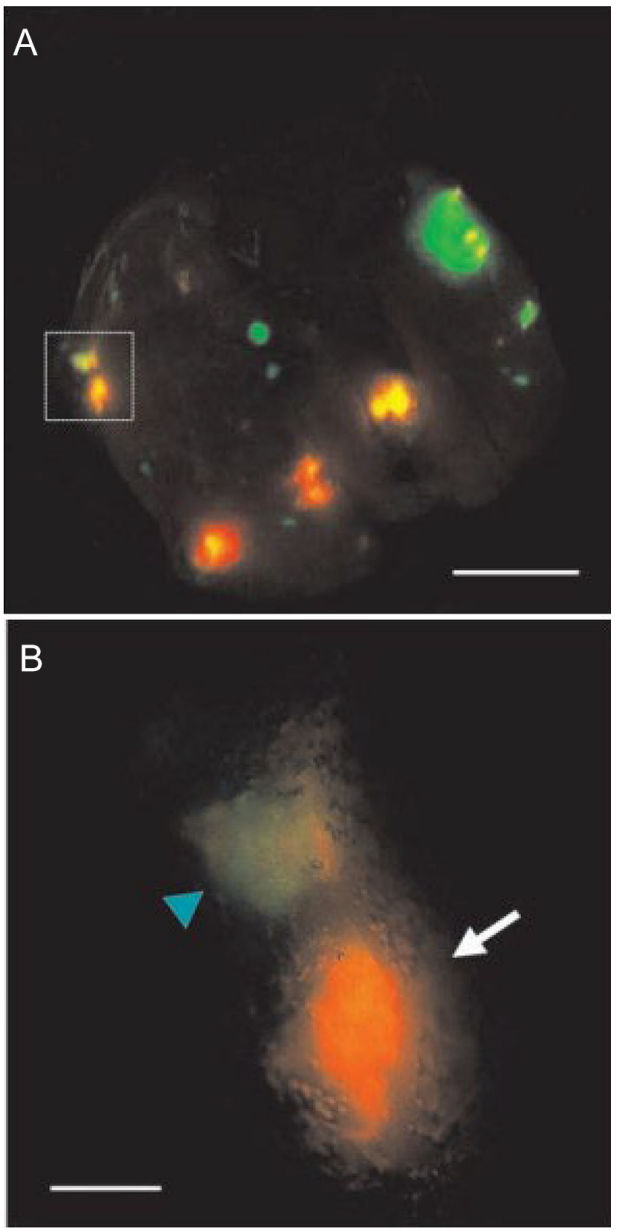

Figure 2. *Determination of the clonal status of lung metastases that occurred spontaneously eight weeks after the co-implantation of HT-1080-GFP and HT-1080-RFP cells in the foot pad. A) Microscopic examination of the removed lung tissue eight weeks after co-injection of HT-1080-GFP cells and HT-1080-RFP cells into the footpad of nude mice, at low magnification. Bar, 5 mm. B) High magnification view of the spontaneous lung metastases shown in A. Bar, 800 μm (17). Most colonies in the lung are one color and, therefore, clonal.*

Post extravasation, Lewis lung cancer (LLC) -GFP-RFP cells remained closely associated with the outer vessel wall and migrated and surrounded the vessel to occupy as much of the vessel surface as possible by elongating their cytoplasm and nuclei (Figure 6A-K) (22).

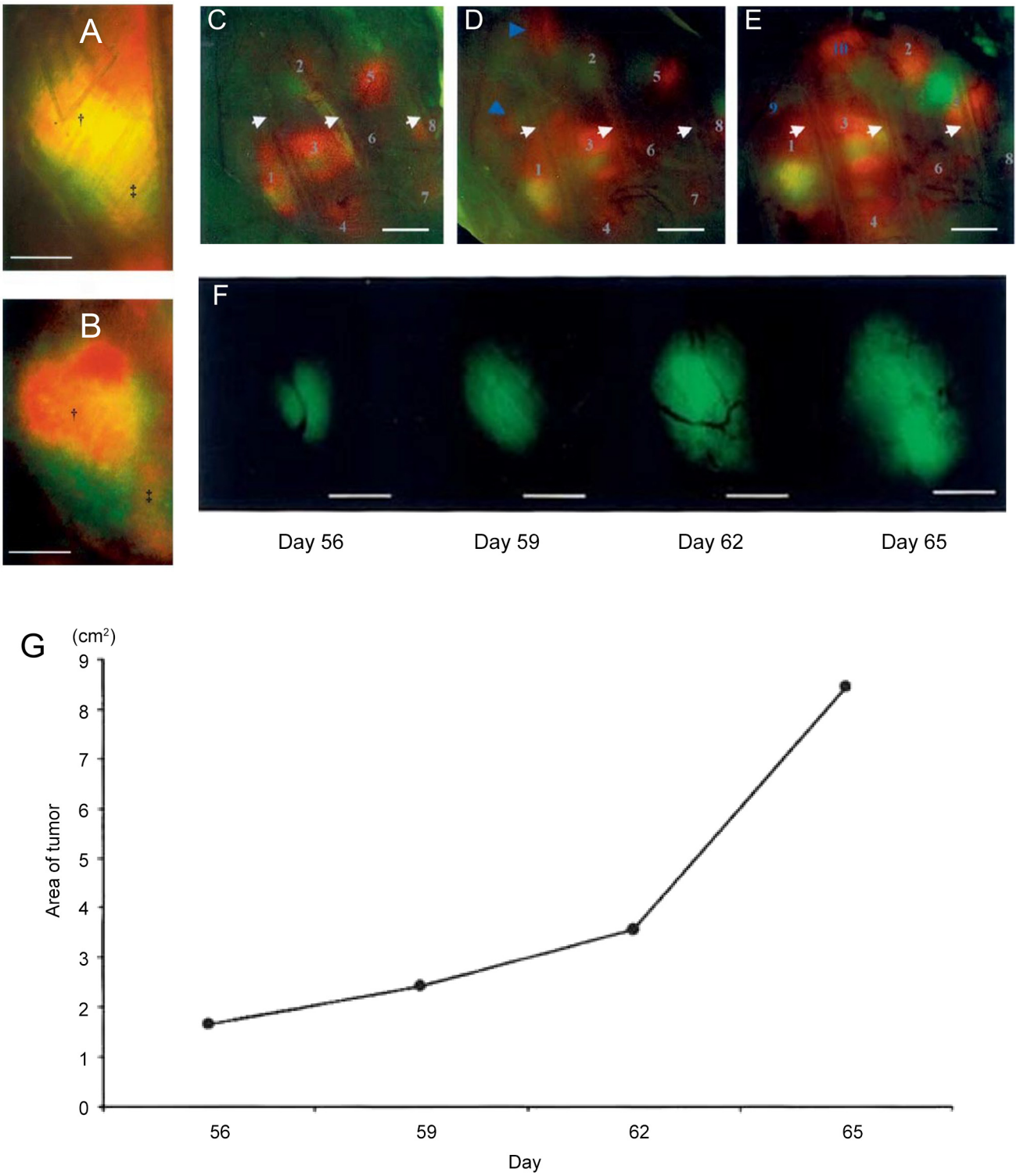

Figure 3. *Real-time imaging of lung metastases in live mice using a skin-flap window for direct imaging. A) Image obtained from a live mouse. B) Image taken from the same mouse after sacrifice, with the chest wall removed. Sequential images capturing the progression of lung micrometastases in a live nude mouse, using spectrally-distinct fluorescent reporters: C) Two weeks after footpad co-injection of HT-1080-GFP and HT-1080-RFP cells (day 15). D) Day 18. E) Day 21. Bars, 2 mm (18). F, G) Sequential images capturing the progression of lung micrometastasis of HT-1080-GFP and HT-1080-RFP cells in a live nude mouse over time. F) Micrometastases were detected using fluorescence microscopy through a skin-flap window starting eight weeks after injection into the footpad (day 56). Bars: 500 μm. G) Area of lung micrometastasis seen in F over-time (19).*

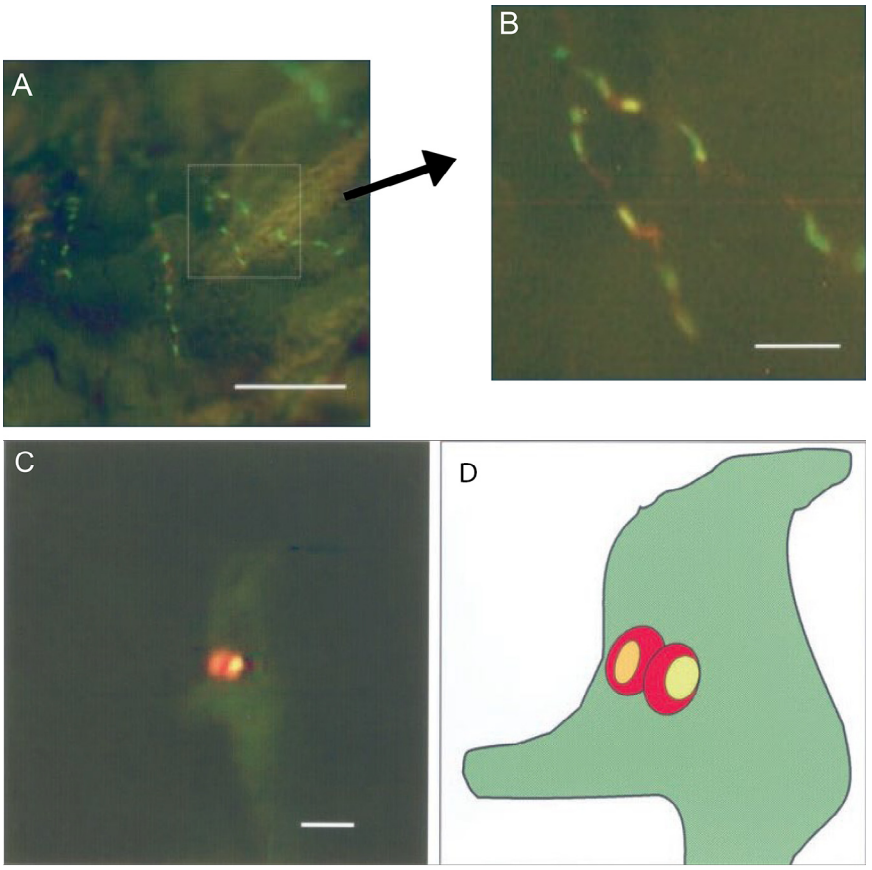

Figure 4. *Live nude mice were used to visualize cancer cells trafficking in the brain. HT-1080-GFP-RFP cells were introduced into the common carotid artery via injection. A) low-magnification view. Bar 400 μm. B) High-magnification view. Bar 100 μm. Live imaging of a mitotic cell in the ear of a live mouse, captured non-invasively in real-time: C) High-magnification non-invasive image. Bar 50 μm. D) Schema of C (20).*

Cyclophosphamide Pre-treatment Enhances Intravascular and Extravascular Growth of Cancer Cells

HT1080 fibrosarcoma cells expressing GFP and RFP died rapidly after injection into the epigastric cranialis vein in an abdominal skin flap made in nude mice. However, if 24 h before cell injection, the mice were pre-treated with the cancer-chemotherapy drug cyclophosphamide, the HT-1080-GFP-RFP cells grew extensively within blood vessels of the cyclophosphamide pre-treated mice and extravasated at high frequency and formed large extravasated colonies. It was speculated that a host-based cancer-cell killing process was inhibited by cyclophosphamide (Figure 7A-L) (23).

Imaging of Nucleolar Dynamics During the Cell Cycle

HT-1080-GFP-RFP cells were seeded on the surface of a skin flap of nude mice, and the cells were imaged 24 h after seeding. The nucleoli of the dual color cells could be imaged very clearly on the surface of the skin flap. The nucleoli were not labeled with GFP or RFP and could be clearly visualized by contrast to the GFP expression in the nucleus. When the cancer cells were in mitosis, the chromatin was highly condensed, and the nucleoli could not be visualized. After mitosis, in early G1, 4 small nucleoli were visualized in each nucleus. During the subsequent phases of the cell cycle, the nucleoli increased in size, but decreased in number. The nucleoli are a potential marker of the cell-cycle phase of cancer cells, which is important since cytotoxic chemotherapy drugs depend on the S-phase of the cell cycle for efficacy (Figure 8A-F, A'-F') (24).

Imaging of the Interaction of Cancer Cells With Immune Cells *In Vivo*

Currently "immuno-oncology" is a very active area of clinical research for the treatment of cancer. Previously, we developed a relevant imageable mouse model to study the

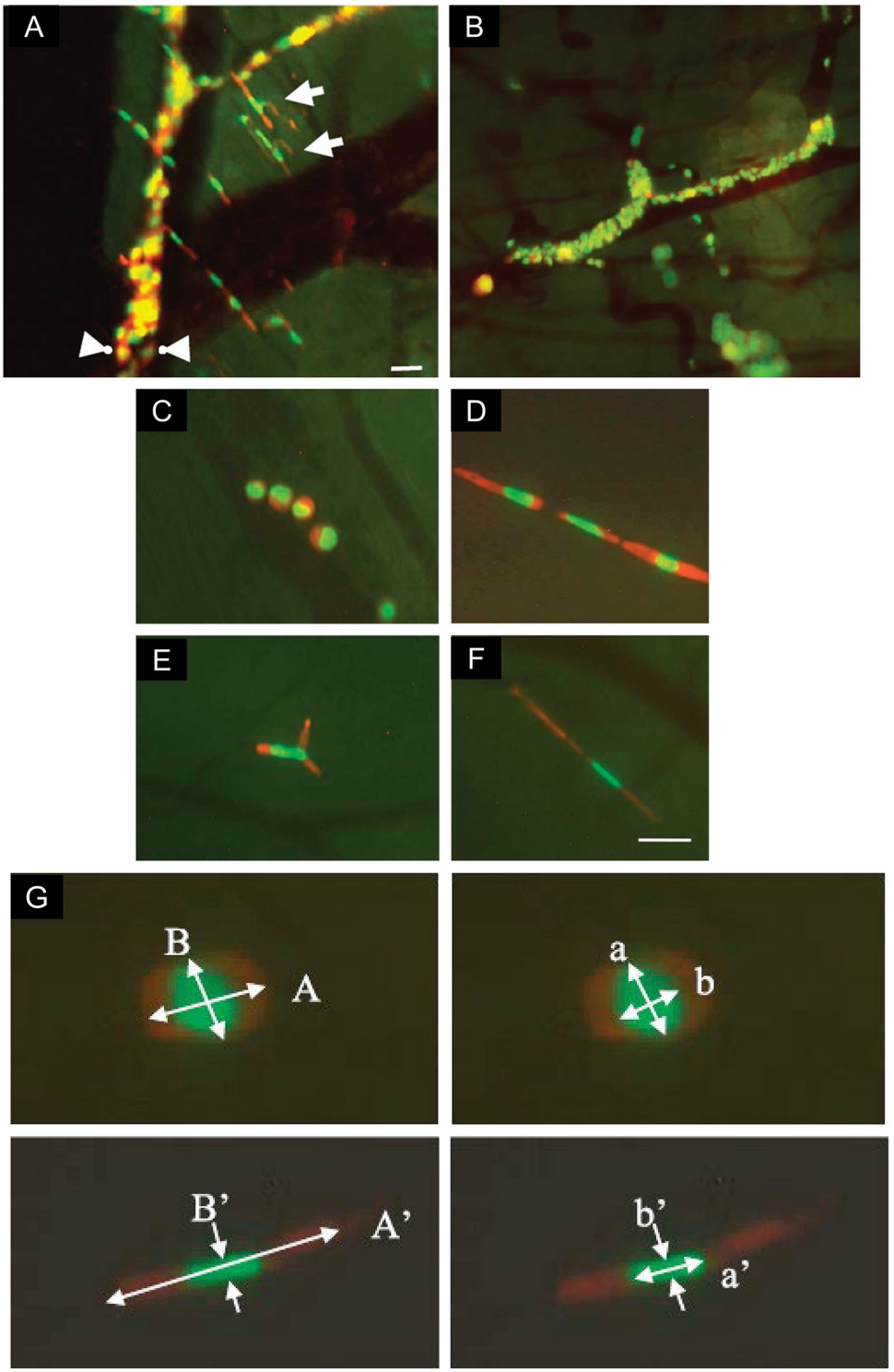

Figure 5. *Cancer cells deform to traffick in narrow capillaries. A, B) Live nude mice were used to visualize HT-1080-GFP-RFP cells in microvessels and capillaries in the skin. A) Following cancer cell injection, the cells were promptly observed within the microvessels and capillaries of the skin flap. B) Immediately following cell injection into a mouse, a large number of circular HT-1080 dual-color cells were observed in the epigastric cranial artery. Bar, 50 μm. C-F) Classification of the deformation of HT-1080-dual-color cells in the vessels in the skin: C) Non-deformed cells are present inside a microvessel. D) The cells and nuclei are stretched to accommodate a capillary. E) The cells are arrested at the point where the capillary divides into two branches. F) Cytoplasmic fragmentation occurs in extremely narrow capillaries; Bar, 50 μm. G) Two examples of before and after nuclear deformation of HT-1080-GFP-RFP cells in a narrow capillary, showing the GFP-expressing nucleus.(21).*

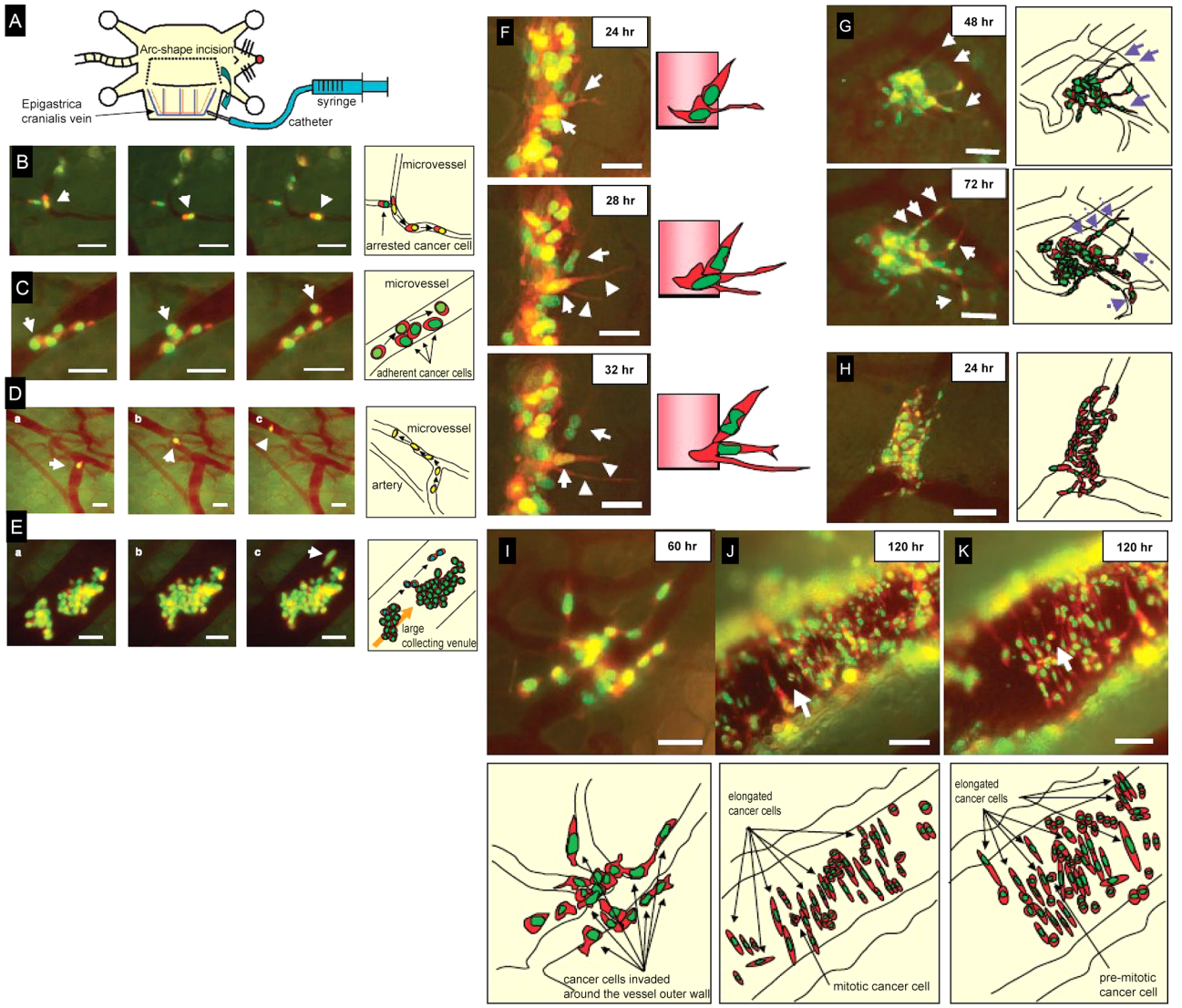

Figure 6. *Real-time trafficking of HT-1080 human fibrosarcoma cells, which are labeled in the nucleus with histone H2B-GFP and in the cytoplasm with RFP, within blood vessels of nude mice and their exit (extravasation) from the blood vessels. A) A schematic diagram illustrating the skin flap model in live mice, which is used for real-time imaging of intravascular trafficking and extravasation. B) The dual-color HT-1080 cells exhibit smooth crawling along the vessel wall in a capillary, without any rolling (arrow). Bar, 100 μm. C) Dual-color HT-1080 cells exhibit low-velocity trafficking as they move between adjacent cells and the vessel wall. Bar, 100 μm. D) A single cancer cell is moving slowly in a capillary. Bar, 50 μm. E) A multicellular aggregate encounters another aggregate that is already adhered to the vessel wall and collides with it. Bar, 100 μm. F-H) Time-lapse imaging was used to observe the process of dual-color MMT mouse mammary tumor cells extravasating. F) 12 h after cell injection. Bar, 20 μm. G) 48 and 72 h after cell injection. Bar, 50 μm. H) The infiltration and rapid multiplication of MMT cells surrounding a blood vessel following extravasation into surrounding tissues. Bar, 50 μm. I, J, K) Visualization of the extravasation, infiltration, and growth of LLC cells using dual-color imaging. I) Extravasated LLC cells exhibit rapid proliferation on the outer wall of the vessel 60 h after injection. J, K) Extravasated LLC cells have spread outside of the blood vessel and wrap around a large vessel 120 h after being injected. Bar, 100 μm (22).*

efficacy of immune-oncology agents. The model used HT1080-GFP-RFP human fibrosarcoma cells and transgenic mice expressing GFP in all immune-cell types. HT-1080-GFP-RFP cells were sprinkled on a skin flap of a GFP-transgenic mouse. After 24 h, GFP-expressing macrophages could be imaged contacting the HT1080-GFP-RFP cells and phagocytizing them. Macrophages could be imaged digesting the HT1080-GFP-RFP cells because RFP cytoplasmic fragments could be visualized within the GFP macrophages. T-cells could kill the dual-color cancer cells by fragmenting them. GFP expressing nuclei of HT1080-GFP-RFP cells which were confronted with T-cells were fragmented and

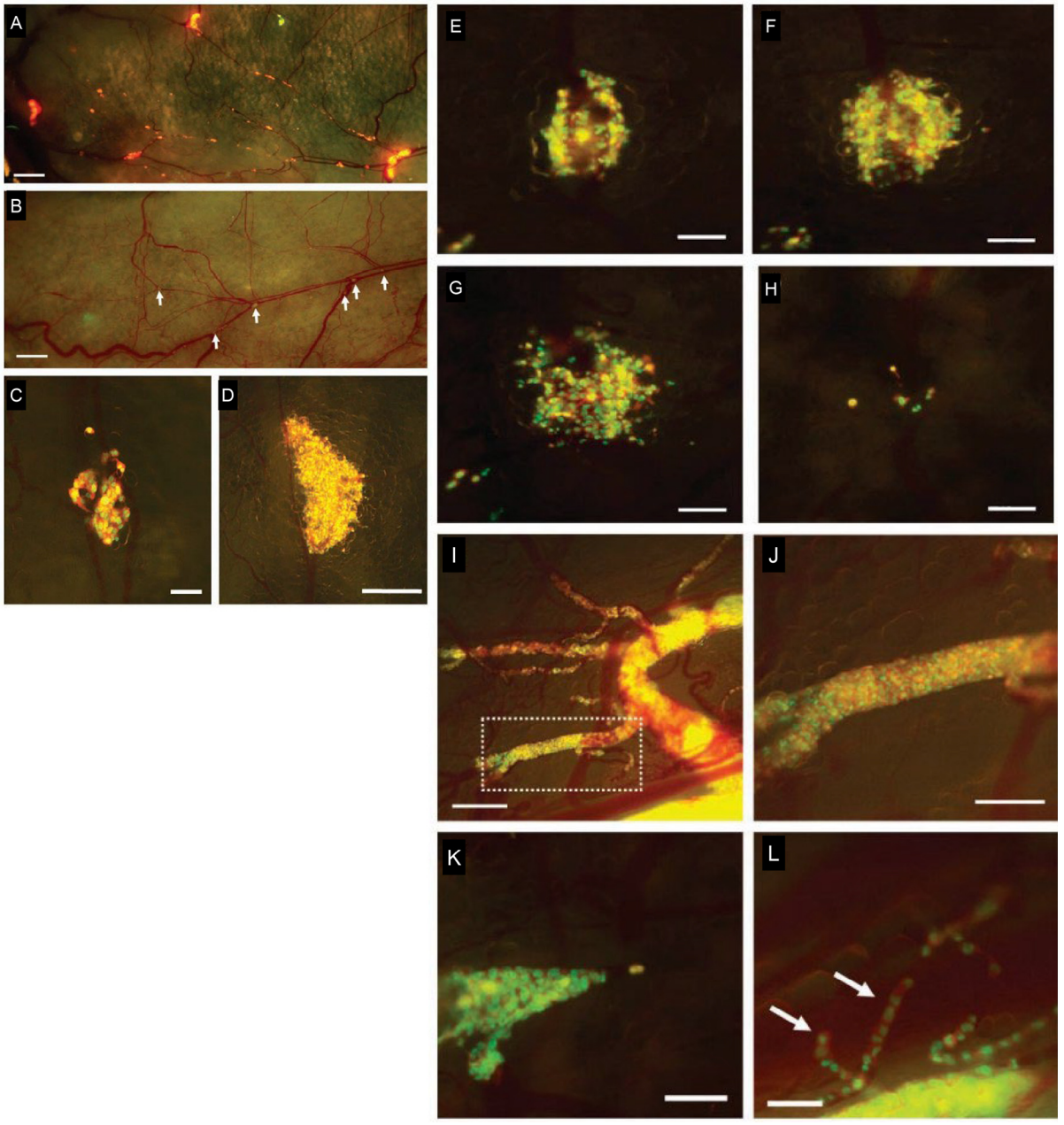

Figure 7. *Effect of cyclophosphamide pre-treatment on cancer-cell colony formation in nude mice imaged in real time. A-D) Fluorescence images of intravascular and extravascular tumor colonies of HT1080 cells labeled with GFP in the nucleus and RFP in the cytoplasm in nude mice that were either pretreated with cyclophosphamide or left untreated. A) Forty-eight hours after injecting dual-color HT1080 cells in the epigastric cranial vein of mice pretreated with cyclophosphamide, numerous fluorescent colonies can be observed both inside and outside the blood vessels. B) In the absence of cyclophosphamide treatment, mice exhibit only a few small tumor thrombi resembling colonies in the blood vessels (indicated by arrows). Bar, 5 mm. C) In mice pre-treated with cyclophosphamide, HT1080 GFP-RFP cells successfully formed compact metastatic colonies following extravasation. Bar, 100 μm. D) In mice pre-treated with cyclophosphamide, a large number of HT1080 cells escaped from blood vessels and formed a cluster around a vessel. Bar, 500 μm. E-H) Time course imaging of HT1080 colony formation and regression after extravasation in cyclophosphamide-pretreated mice. E) Four days after injection of HT1080 GFP-RFP cells, a large number of cells formed a metastatic colony around blood vessels following extravasation. F) By day 6, the cells underwent rapid proliferation and infiltration around the vessel, resulting in a significant increase in the size of the colony. G) A significant proportion of the cells disappeared, while numerous cells assumed a rounded shape by day 7. H) On day 9, there are only seven remaining cells, all of which are spherical in shape. Bar, 200 μm. I-L) Temporal imaging of the growth and dissemination of HT1080 cells within blood vessels in nude mice pre-treated with cyclophosphamide. I) 14 days after cell injection, HT1080 GFP-RFP cells invaded and multiplied within the blood vessels without extravasating. Bar, 2 mm. J) Enlarged image as indicated. Bar, 500 μm. K) On day 7 after cell injection of HT1080 GFP-RFP cells, a significant number of cells occupied the vessel. Bar, 200 μm. L) The HT1080 GFP-RFP cells exhibited limited migration within capillaries. Bar, 100 μm (23).*

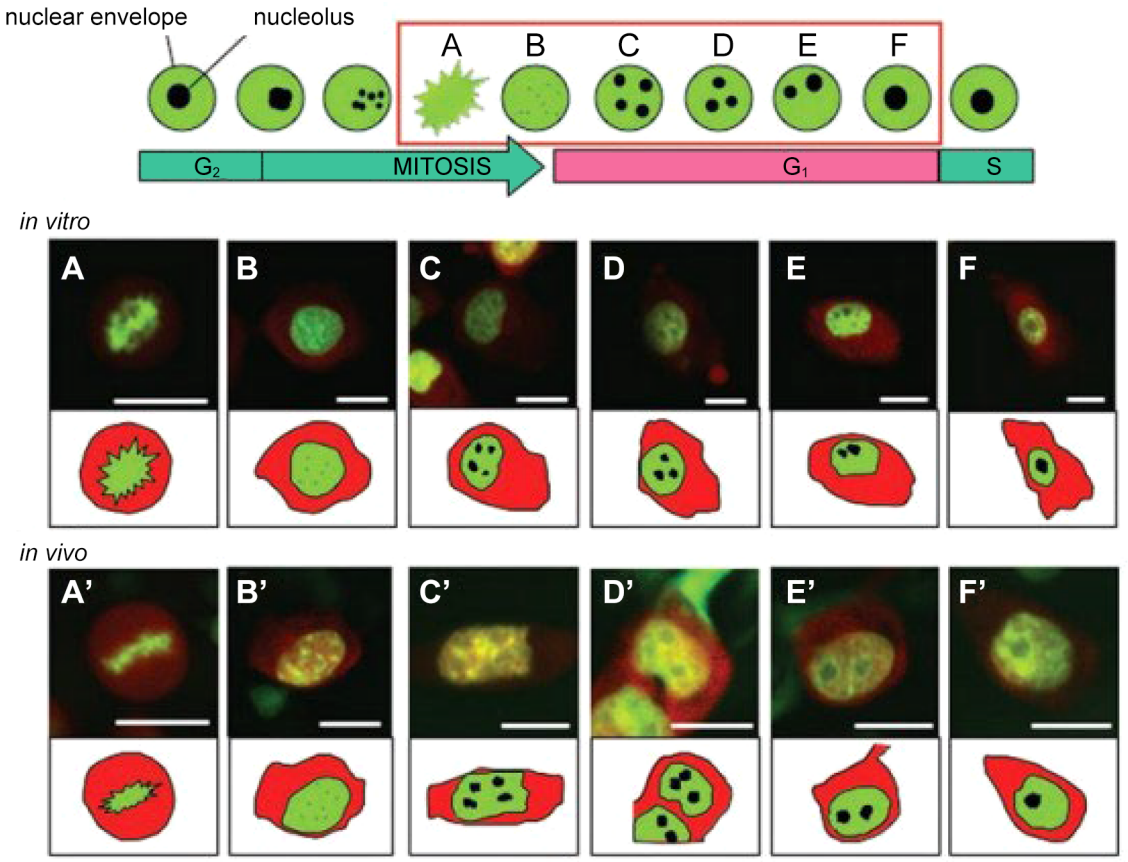

Figure 8. *Observation of nucleolar dynamics in real-time throughout the cell cycle in vitro and in vivo of HT1080-GFP-RFP fibrosarcoma cells. A and A') During the process of mitosis, the HT1080 GFP-RFP cells underwent chromatin condensation, resulting in the nucleolus becoming unobservable. B and B') Following mitosis, the nuclei assumed a spherical shape. C and C') During the early G1 phase, four nucleoli are observed within each nucleus. D, D', F and F') The nucleoli exhibited a lighter appearance compared to the GFP expressed in the nucleus and remained*

appeared to be at an early stage of apoptosis. This model can be used to determine whether immuno-oncology agents, such as immune check-point inhibitors, could enhance caner-cell killing (Figure 9A-J) (25).

Imaging Real-time Shedding and Trafficking of Cancer Cells in Lymphatic Channels

Lymphatic trafficking is a common route of metastatic spread of HT1080-GFP-RFP fibrosarcoma cells. In one experiment HT1080-GFP-RFP cells were injected into nude mice in the inguinal lymph node in a skin flap, along with FITC dextran to label lymphatic channels, enabling the imaging of labeled cancer cells in lymphatic channels. The cancer cells could be imaged later in the axillary lymph nodes, also labeled with FITC dextran. Spontaneous lymphatic trafficking of cancer cells was also observed, after HT-1080-GFP-RFP cells were injected into the footpad of mice from where they subsequently metastasized to the popliteal lymph node. When the metastatic popliteal lymph node was exposed, dual-color cancer cell trafficking in lymphatic channels connected to the metastatic lymph node could be imaged. When 25 g or 100 g weights were applied to a footpad tumor formed from HT-1080-RFP-GFP cells, cancer cells were imaged shedding in the lymphatic channel leading to the popliteal lymph node, with the greater weight causing much more cancer-cell shedding than the lesser weight (Figure 10A-N) (26).

Imaging Single Cancer-cell Dynamics of Metastasis to the Lung in Real Time

In order to image the trafficking of cancer cells to the lung, the chest wall of the nude mouse had to be open for long periods. Thus, assisted breathing was necessary to keep the mice alive. Therefore, a novel retrograde wire-guided endotracheal intubation procedure for mice was developed. An intravenous catheter of 25 mm length was used as an

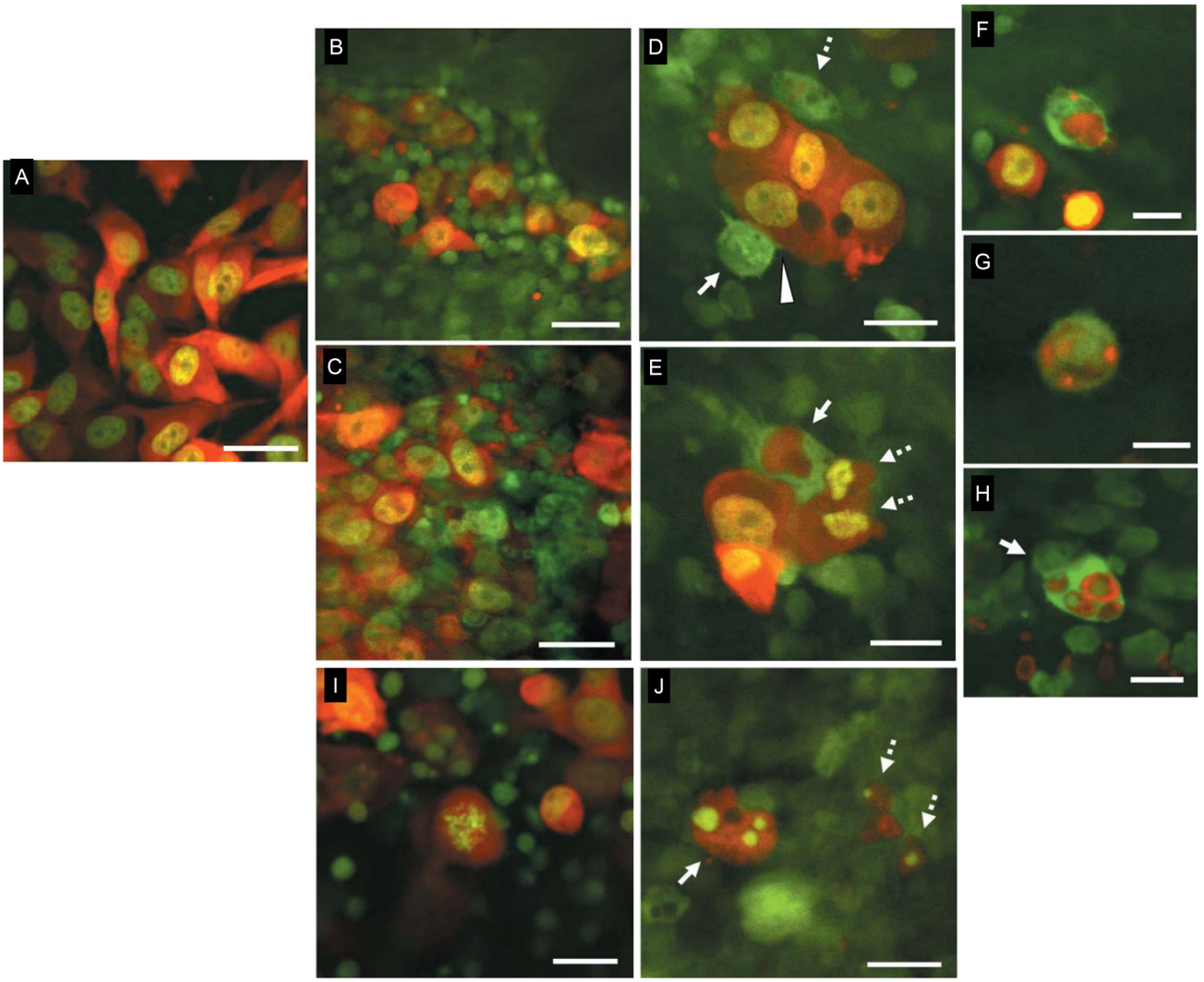

Figure 9. *Real-time imaging of cancer-cell immune-cell interaction in vivo. A) Green fluorescent protein (GFP)- and red fluorescent protein (RFP)-expressing human fibrosarcoma cells (HT-1080-GFP-RFP cells) in vitro. Bar, 50 μm. B) Lymphocytes from transgenic C57/B6-GFP mice can be observed surrounding HT-1080-GFP-RFP cells. C) Many lymphocytes and macrophages expressing GFP from the host cells, interacting with HT-1080-GFP-RFP cell aggregates. Bar, 50 μm. Live transgenic C57/B6-GFP mice were used to visualize the interaction between host macrophages and cancer cells. D) The GFP macrophages were observed making contact with HT-1080-GFP-RFP cells (indicated by an arrow and a broken arrow). E) A macrophage is observed engulfing the cytoplasm of an HT-1080-GFP-RFP cell. Bar, 20 μm. F-H) Imaging a macrophage phagocytosing a cancer cell in live transgenic C57/B6-GFP mice. F) Within the macrophage, a portion of cytoplasm containing RFP, derived from an HT-1080-GFP-RFP cell, is observable. G) The cytoplasm of an HT-1080-GFP-RFP cell, which contained the RFP protein, was broken down and fragmented by a macrophage. H) The macrophage phagocytosed four HT-1080-GFP-RFP cells simultaneously. Bar, 20 μm. I-J) Live transgenic C57/B6-GFP mice were used to visualize the process of lymphocyte-mediated cancer-cell killing. I) Within 24 h of transplanting HT-1080-GFP-RFP cells, the nucleus containing GFP was observed to be fragmented within a single cell. J) The GFP nucleus in the HT-1080 cell underwent fragmentation into three distinct parts, as indicated by the arrow. Bar, 20 μm (25).*

endotracheal tube. A guide wire was inserted into the trachea through a small hole. The endotracheal catheter could then be accurately introduced into the trachea over the guide wire. The intubation tube was connected to an oxygen tube. At this point, the chest wall could be opened. Anesthesia was maintained with isoflurane applied *via* a vaporizer. A positive end expiratory pressure (PEEP) system was used to regulate lung inflation and deflation. After each imaging session, the chest wall was closed with 6-0 sutures. Imaging sessions were carried out for as long as 8 h and repeated up to 6 times per mouse. Cancer cells expressing GFP in the nuclei and RFP in the cytoplasm were injected into the tail vein, and HT1080-

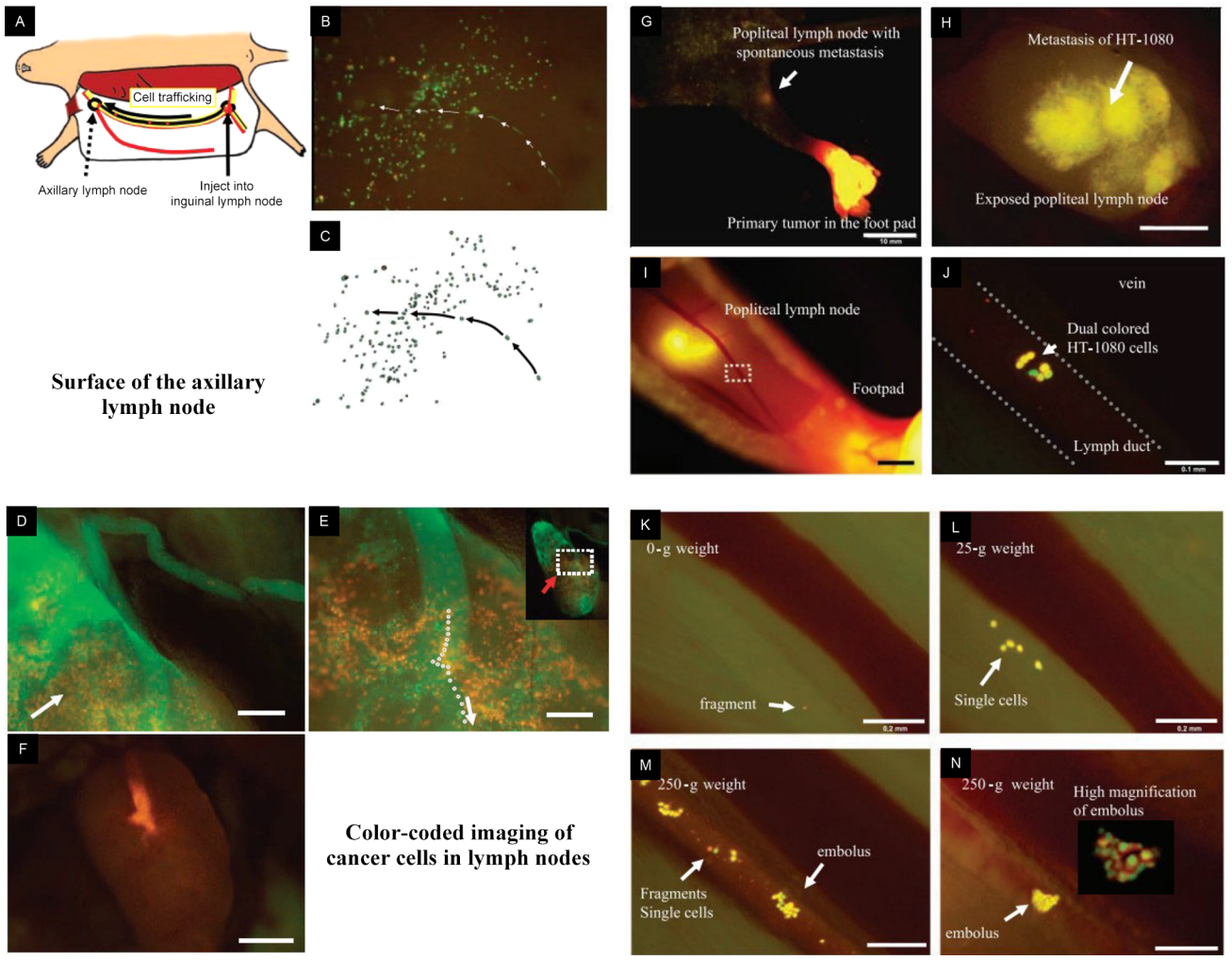

Figure 10. *Imaging of lymphatic trafficking of cancer cells in real time. A-C) An experimental nude-mouse model was developed to image lymph-node metastasis, specifically the migration of cancer cells from the inguinal lymph node to the axillary lymph node after injection. A) HT-1080 GFP-RFP human fibrosarcoma cells were introduced into the inguinal lymph node. B) Cancer cells infiltrating the axillary lymph node through the afferent lymphatic duct. C) schematic of (A). D-F) Imaging of both lymphatic structure and the trafficking of cancer cells. D) The fluorescence of FITC-dextran (green) shows the anatomical arrangement of the lymphatic system and the axillary lymph node. Bar, 500 μm. E) Trafficking of individual cells occurs at the point where an afferent lymph duct meets the subcapsular sinus of the lymph node. Bar, 200 μm. F) 5×10^5 XPA1-RFP human pancreatic cancer cells were injected into the inguinal lymph node, and the axillary lymph node was imaged 7 days later. Bar, 1 mm. G-J) Nude-mouse model for the spontaneous metastasis of cancer cells injected into the footpad. G) HT-1080 GFP-RFP cells were injected into the footpad. H) Fluorescence image of an exposed popliteal lymph node in (G). I) A visible popliteal lymph node. J) Movement of HT-1080 dual-color cells in the lymphatic system, which is indicated by dotted lines. Bar, 10 mm (G); 1 mm (H); 2 mm (I); and 100 μm (J). K-N) The impact of tumor pressure on the shedding of cancer cells into lymphatic vessels. K) No pressure or force was applied to the footpad. L) Following a 10-second stimulation with a 25-gram weight on the footpad, both individual HT-1080 GFP-RFP cells and fragments of HT-1080 GFP-RFP cells can be observed moving through the lymph duct. M and N) Following a 10 s stimulation with a 250 g weight on the footpad, there was an increased shedding of cancer-cell emboli, individual cancer cells, and fragments of cancer cells into the lymph duct. Bar, 200 μm (K-N) (26).*

GFP-RFP or MMT-GFP-RFP cells could be imaged arriving to the lung in real time. Surviving cells in the lung could be imaged to form colonies in the lung with multiple imaging sessions over 10 days. Only rare cells among these arriving in the lung after tail vein injection could survive and form colonies in the lung (Figure 11A-Q) (27).

Imaging Bone Marrow Metastasis by Prostate Cancer Cells in Real Time

PC-3 human prostate cancer cells were injected into the heart ventricle of nude mice. Subsequently multiple metastasis were observed in the skull, femur, rib, and

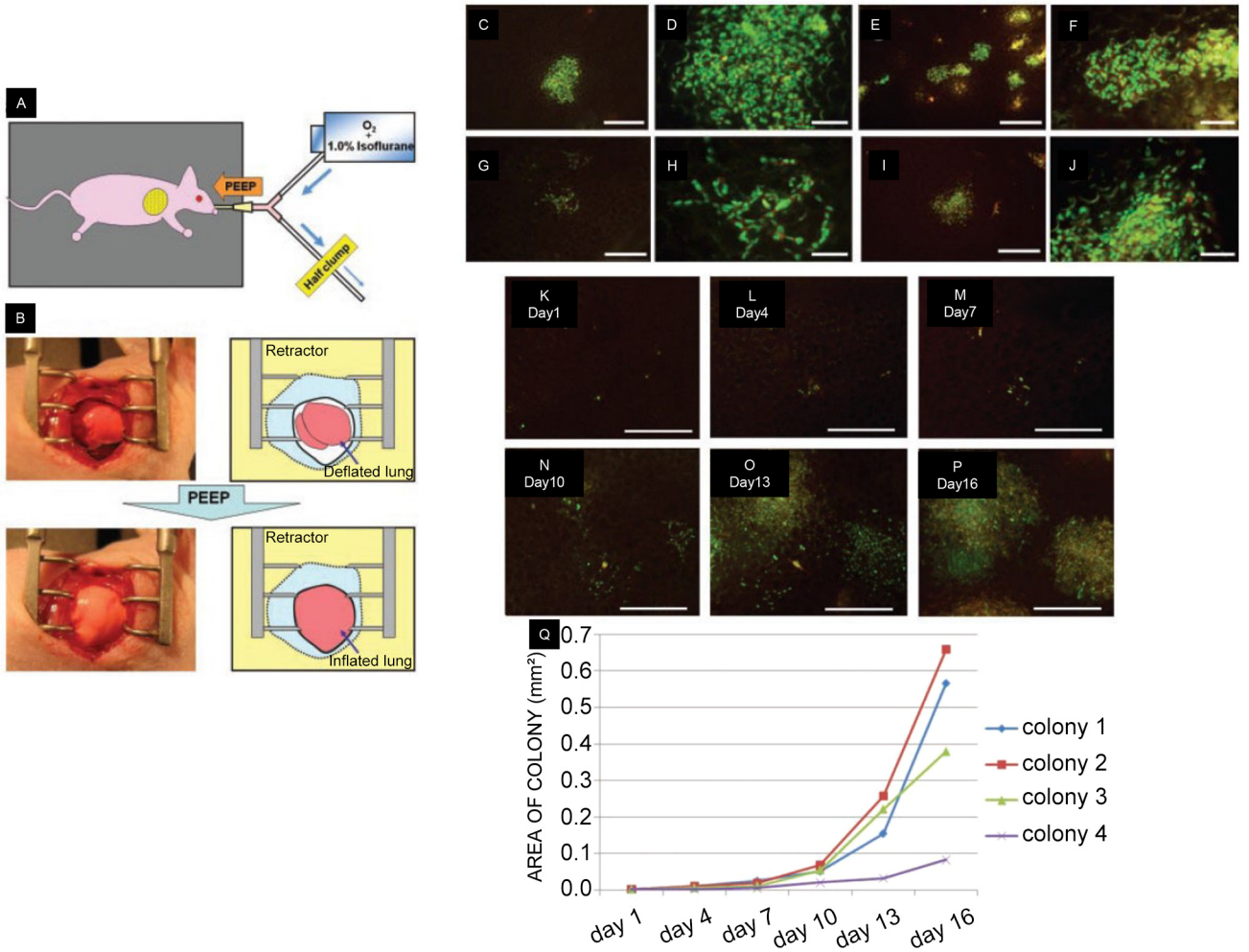

Figure 11. *Imaging of cancer-cell trafficking and colony formation in the lung in real-time. A, B) Ventilation system for open-chest images of cancer cells trafficking to the lung of nude mice. A) A tracheal tube was secured to a Y-shaped connector, and an exhaust tube was connected to one of the ends. B) Upon opening the chest wall, the lung promptly collapsed. C-J) Visualization of the morphology of lung colonies formed by HT1080 GFP-RFP cells. C-F) The lung contains metastatic colonies of HT1080 GFP-RFP cells. D) High magnification image of (C). F) High magnification image of (E). G-J) Lung metastases of murine mammary carcinoma (MMT) cells expressing GFP in the nucleus and RFP in the cytoplasm. H) High magnification image of (G). J) High magnification image of (I). C, E, G, I) Scale bar, 500 mm. D, F, H, J) Scale bar, 100 mm. K-Q) Temporal imaging of cancer-cell colony development in the lung of live mice. K-P) On day 0, a total of $2x10^5$ MMT GFP-RFP cells were injected into the tail vein of nude mice. Scale bar, 500 mm. Q) Proliferation rates of colonies of dual-color MMT cells in the lung (27).*

vertebral bones. Time-course imaging *via* skin flaps demonstrated the formation of metastatic colonies in the bones. Twenty min after cardiac injection of PC-3 GFP cells in RFP transgenic mice, the PC-3-GFP cells could be imaged at the single-cell level in the bone marrow of the skull.

After intra-tibial injection of PC-3 cells, RFP-expressing PC-3 cells were imaged growing in the bone marrow and spreading to an inguinal lymph node. This model can thus be used to image the lethal aspect of prostate cancer, metastasis to the bone (Figure 12A-C) (28).

Discussion

Exquisite application of experimental microsurgery and fluorescent genetic reporters enabled the establishment of unique mouse models of cancer, that along with appropriate imaging technologies, could be used to visualize all the critical aspects of cancer progression, in particular the mechanism of metastatic spread at the single-cell or sub-cellular level that distinguished the cellular cytoplasm and nuclei *in vivo*.

Imaging of the cancer cells was enabled by their strong expression of GFP and RFP, including the capability of

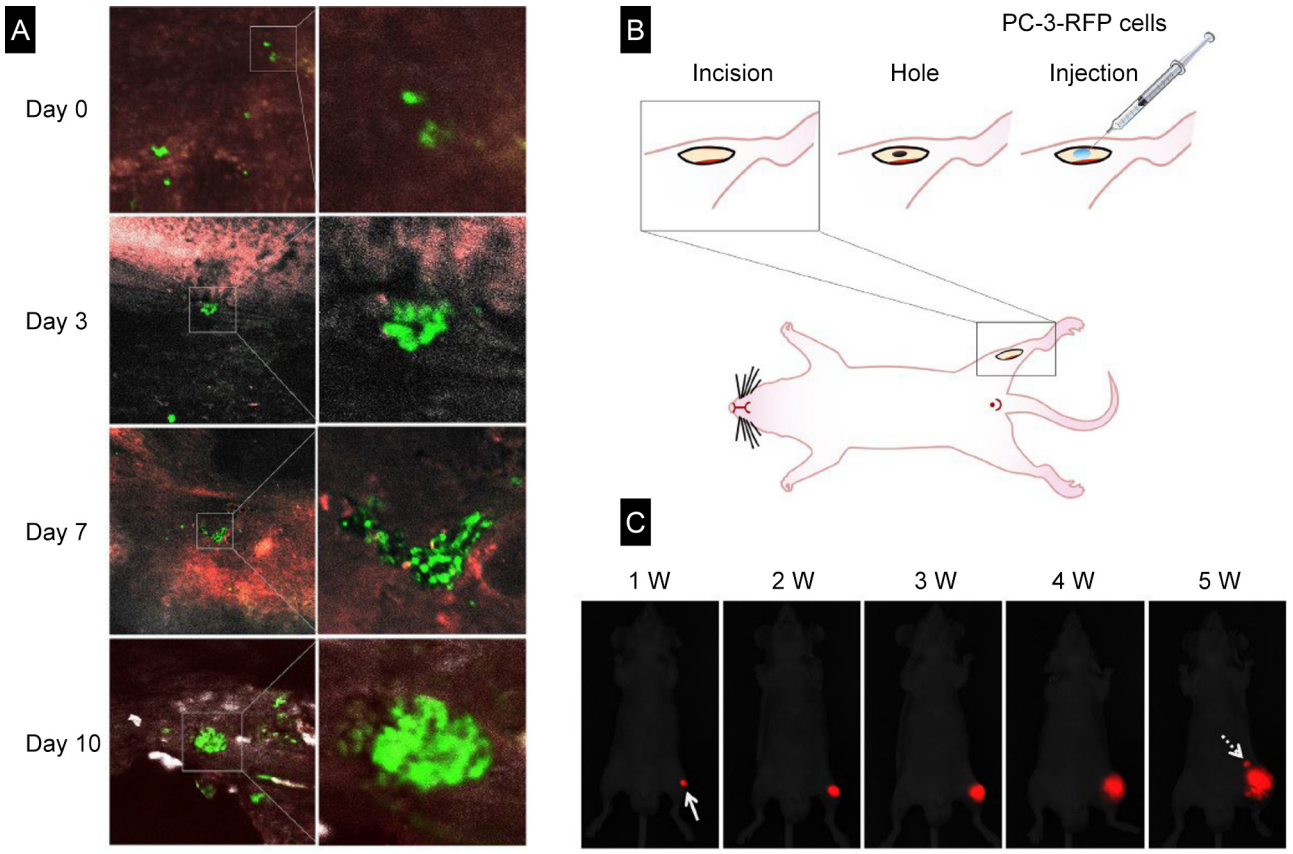

Figure 12. *Real-time imaging of prostate cancer-cell metastatic progression. A) Fluorescence imaging was used to track the progression of PC-3-GFP-BM6 micrometastases in the bone marrow of nude mice at the cellular level over time. Real-time fluorescence imaging was used to track the progression of a single bone metastasis following the injection of PC-3-RFP into the tibia. Left-side panels are low magnifications and right-side panels are high magnification. B) schema of how PC-3-RFP cells were introduced into the tibia of nude mice. C) Temporal non-invasive fluorescence imaging of a single bone metastasis (28).*

cancer cells to deform and traffic in narrow vessels, extravasate, and subsequently form colonies in distant organs, all of which are the most critical steps of metastases.

Real-time in vivo imaging demonstrated the interaction of cancer cells and immune cells which can be a model of the mode of action of immune checkpoint inhibitors (ICI).

The models described in this brief perspective represent a revolutionary and disruptive improvement over previous cancer models. The unique collaboration of young physician-scientists from Kanazawa University, AntiCancer Inc., and UCSD made this possible.

Conflicts of Interest

The Authors declare no competing interests.

Authors' Contributions

SM, NY, and RMH wrote the paper. KY, KH, HK, SM, KI, TH, HT, and SD critically read and approved the final manuscript.

Acknowledgements

This paper is dedicated to the memory of A. R. Moossa, MD, Sun Lee, MD, Professor Gordon H. Sato, Professor Li Jiaxi, Masaki Kitajima, MD, Shigeo Yagi, PhD, Jack Geller, MD, Joseph R. Bertino, MD, J.A.R. Mead PhD, Eugene P. Frenkel, MD, Professor Sheldon Penman, Professor John R. Raper and Joseph Leighton, MD.

References

1 Rygaard J, Povlsen CO: Heterotransplantation of a human malignant tumour to "Nude" mice. Acta Pathol Microbiol Scand 77(4): 758-760, 1969. DOI: 10.1111/j.1699-0463.1969.tb04520.x

2 Hoffman RM: Patient-derived mouse models of cancer. New York, NY, USA, Humana Press, 2017. DOI: 10.1007/978-3-319-57424-0

3 Sordat BCM, Ueyama Y, Fogh J: Metastasis of tumor xenografts in the nude mice. *In*: The Nude Mouse in Experimental and Clinical Research. Fogh J, Giovanella BC (eds.). Academic press, 1978.

4 Hoffman RM: Patient-derived orthotopic xenografts: better mimic of metastasis than subcutaneous xenografts. Nat Rev Cancer 15(8): 451-452, 2015. DOI: 10.1038/nrc3972

5 Lee S: Experimental Microsurgery. Tokyo, Igaku-Shoin Medical Publishers, 1987.
6 Fu X, Theodorescu D, Kerbel RS, Hoffman RM: Extensive multi-organ metastasis following orthotopic onplantation of histologically-intact human bladder carcinoma tissue in nude mice. Int J Cancer 49(6): 938-939, 1991. DOI: 10.1002/ijc.2910490623
7 Fu X, Hoffman RM: Human RT-4 bladder carcinoma is highly metastatic in nude mice and comparable to ras-H-transformed RT-4 when orthotopically onplanted as histologically intact tissue. Int J Cancer 51(6): 989-991, 1992. DOI: 10.1002/ijc.2910510625
8 Wang X, Fu X, Hoffman RM: A new patient-like metastatic model of human lung cancer constructed orthotopically with intact tissue *via* thoracotomy in immunodeficient mice. Int J Cancer 51(6): 992-995, 1992. DOI: 10.1002/ijc.2910510626
9 Fu X, Le P, Hoffman RM: A metastatic orthotopic-transplant nude-mouse model of human patient breast cancer. Anticancer Res 13(4): 901-904, 1993.
10 Fu X, Hoffman RM: Human ovarian carcinoma metastatic models constructed in nude mice by orthotopic transplantation of histologically-intact patient specimens. Anticancer Res 13(2): 283-286, 1993.
11 Fu X, Guadagni F, Hoffman RM: A metastatic nude-mouse model of human pancreatic cancer constructed orthotopically with histologically intact patient specimens. Proc Natl Acad Sci USA 89(12): 5645-5649, 1992. DOI: 10.1073/pnas.89.12.5645
12 Fu XY, Besterman JM, Monosov A, Hoffman RM: Models of human metastatic colon cancer in nude mice orthotopically constructed by using histologically intact patient specimens. Proc Natl Acad Sci USA 88(20): 9345-9349, 1991. DOI: 10.1073/pnas.88.20.9345
13 Fu X, Herrera H, Hoffman RM: Orthotopic growth and metastasis of human prostate carcinoma in nude mice after transplantation of histologically intact tissue. Int J Cancer 52(6): 987-990, 1992. DOI: 10.1002/ijc.2910520626
14 Chishima T, Miyagi Y, Wang X, Yamaoka H, Shimada H, Moossa AR, Hoffman RM: Cancer invasion and micrometastasis visualized in live tissue by green fluorescent protein expression. Cancer Res 57(10): 2042-2047, 1997.
15 Yang M, Baranov E, Jiang P, Sun FX, Li XM, Li L, Hasegawa S, Bouvet M, Al-Tuwaijri M, Chishima T, Shimada H, Moossa AR, Penman S, Hoffman RM: Whole-body optical imaging of green fluorescent protein-expressing tumors and metastases. Proc Natl Acad Sci USA 97(3): 1206-1211, 2000. DOI: 10.1073/pnas.97.3.1206
16 Yamamoto N, Yang M, Jiang P, Xu M, Yamauchi K, Tsuchiya H, Tomita K, Moossa AR, Hoffman RM: Color coding cancer cells with fluorescent proteins to visualize *in vivo* cellular interaction in metastatic colonies. Anticancer Res 24(6): 4067-4072, 2004.
17 Yamamoto N, Yang M, Jiang P, Xu M, Tsuchiya H, Tomita K, Moossa AR, Hoffman RM: Determination of clonality of metastasis by cell-specific color-coded fluorescent-protein imaging. Cancer Res 63(22): 7785-7790, 2003.
18 Yamamoto N, Yang M, Jiang P, Xu M, Tsuchiya H, Tomita K, Moossa AR, Hoffman RM: Real-time imaging of individual fluorescent-protein color-coded metastatic colonies *in vivo*. Clin Exp Metastasis 20(7): 633-638, 2003. DOI: 10.1023/a:1027311230474
19 Yamamoto N, Yang M, Jiang P, Tsuchiya H, Tomita K, Moossa AR, Hoffman RM: Real-time GFP imaging of spontaneous HT-1080 fibrosarcoma lung metastases. Clin Exp Metastasis 20(2): 181-185, 2003. DOI: 10.1023/a:1022662927574
20 Yamamoto N, Jiang P, Yang M, Xu M, Yamauchi K, Tsuchiya H, Tomita K, Wahl GM, Moossa AR, Hoffman RM: Cellular dynamics visualized in live cells *in vitro* and *in vivo* by differential dual-color nuclear-cytoplasmic fluorescent-protein expression. Cancer Res 64(12): 4251-4256, 2004. DOI: 10.1158/0008-5472.CAN-04-0643
21 Yamauchi K, Yang M, Jiang P, Yamamoto N, Xu M, Amoh Y, Tsuji K, Bouvet M, Tsuchiya H, Tomita K, Moossa AR, Hoffman RM: Real-time *in vivo* dual-color imaging of intracapillary cancer cell and nucleus deformation and migration. Cancer Res 65(10): 4246-4252, 2005. DOI: 10.1158/0008-5472.CAN-05-0069
22 Yamauchi K, Yang M, Jiang P, Xu M, Yamamoto N, Tsuchiya H, Tomita K, Moossa AR, Bouvet M, Hoffman RM: Development of real-time subcellular dynamic multicolor imaging of cancer-cell trafficking in live mice with a variable-magnification whole-mouse imaging system. Cancer Res 66(8): 4208-4214, 2006. DOI: 10.1158/0008-5472.CAN-05-3927
23 Yamauchi K, Yang M, Hayashi K, Jiang P, Yamamoto N, Tsuchiya H, Tomita K, Moossa AR, Bouvet M, Hoffman RM: Induction of cancer metastasis by cyclophosphamide pretreatment of host mice: an opposite effect of chemotherapy. Cancer Res 68(2): 516-520, 2008. DOI: 10.1158/0008-5472.CAN-07-3063
24 Yamauchi K, Yang M, Hayashi K, Jiang P, Yamamoto N, Tsuchiya H, Tomita K, Moossa AR, Bouvet M, Hoffman RM: Imaging of nucleolar dynamics during the cell cycle of cancer cells in live mice. Cell Cycle 6(21): 2706-2708, 2007. DOI: 10.4161/cc.6.21.4861
25 Yamauchi K, Tome Y, Yamamoto N, Hayashi K, Kimura H, Tsuchiya H, Tomita K, Bouvet M, Hoffman RM: Color-coded real-time subcellular fluorescence imaging of the interaction between cancer and host cells in live mice. Anticancer Res 32(1): 39-43, 2012.
26 Hayashi K, Jiang P, Yamauchi K, Yamamoto N, Tsuchiya H, Tomita K, Moossa AR, Bouvet M, Hoffman RM: Real-time imaging of tumor-cell shedding and trafficking in lymphatic channels. Cancer Res 67(17): 8223-8228, 2007. DOI: 10.1158/0008-5472.CAN-07-1237
27 Kimura H, Hayashi K, Yamauchi K, Yamamoto N, Tsuchiya H, Tomita K, Kishimoto H, Bouvet M, Hoffman RM: Real-time imaging of single cancer-cell dynamics of lung metastasis. J Cell Biochem 109(1): 58-64, 2010. DOI: 10.1002/jcb.22379
28 Miwa S, Toneri M, Igarashi K, Yano S, Kimura H, Hayashi K, Yamamoto N, Tsuchiya H, Hoffman RM: Real-time *in vivo* confocal fluorescence imaging of prostate cancer bone-marrow micrometastasis development at the cellular level in nude mice. J Cell Biochem 117(11): 2533-2537, 2016. DOI: 10.1002/jcb.25545

Received May 21, 2024
Revised June 18, 2024
Accepted June 19, 2024